metals

MDPI

Article

Experimental Determination of the Standard Gibbs Energy of Formation of $Fe_{3-x}V_xO_4$ at 1473 K

Qingdong Miao [1], Ming Li [1] and Baijun Yan [2,3,*]

[1] State Key Laboratory for Comprehensive Utilization of Vanadium and Titanium Resources, Pangang Group Institute Co., Ltd., Panzhihua 617000, China; mqd2002041@126.com (Q.M.); liming00929@163.com (M.L.)
[2] State Key Laboratory of Advanced Metallurgy, Beijing 100083, China
[3] School of Metallurgical and Ecological Engineering, University of Science and Technology Beijing, Beijing 100083, China
* Correspondence: baijunyan@ustb.edu.cn

Abstract: In the present study, an approach of determining the standard Gibbs energy of formation of $Fe_{3-x}V_xO_4$ was proposed firstly, then the standard Gibbs energies of formation of a variety of $Fe_{3-x}V_xO_4$ were determined experimentally, and finally, a calculating model of the standard Gibbs energy of formation of $Fe_{3-x}V_xO_4$ was established. The detailed results are as follows: (1) the standard Gibbs energy of formation of $Fe_{3-x}V_xO_4$ can be determined successfully by two steps; the first is to measure the chemical potential of Fe in $Fe_{3-x}V_xO_4$ under fixed oxygen partial pressure, the second is to derive the chemical potential of V in $Fe_{3-x}V_xO_4$ by Gibbs–Duhem relation; (2) the standard Gibbs energies of formation of $Fe_{3-x}V_xO_4$ are mainly decided by the Fe/V molar ratio, and almost not influenced by the oxygen partial pressure in the range from 2.39×10^{-12} to 3.83×10^{-11} atm; (3) in this oxygen partial pressure range, the standard Gibbs energies of formation of $Fe_{3-x}V_xO_4$ can be calculated satisfactorily by the following model: $\Delta_f G^{\theta}_{Fe_{3-x}V_xO_4}(J/mol) = (1-x/2)\Delta_f G^{\theta}_{Fe_3O_4} + (x/2)\Delta_f G^{\theta}_{FeV_2O_4} + (1-x/2)RTln(1-x/2) + (x/2)RTln(x/2) - 168627.48(1-x/2)(x/2)$.

Keywords: $Fe_{3-x}V_xO_4$; Gibbs energy; measurement; modeling; Gibbs–Duhem relation

check for updates

Citation: Miao, Q.; Li, M.; Yan, B. Experimental Determination of the Standard Gibbs Energy of Formation of $Fe_{3-x}V_xO_4$ at 1473 K. *Metals* **2023**, *13*, 1498. https://doi.org/10.3390/met13081498

Academic Editor: Andrii Kostryzhev

Received: 3 July 2023
Revised: 1 August 2023
Accepted: 16 August 2023
Published: 21 August 2023

Copyright: © 2023 by the authors. Licensee MDPI, Basel, Switzerland. This article is an open access article distributed under the terms and conditions of the Creative Commons Attribution (CC BY) license (https://creativecommons.org/licenses/by/4.0/).

1. Introduction

The Fe–V–O system has attracted huge interest for decades due to the variety of the iron vanadate oxides formed in this system and the diverse applications of the oxides [1,2]. For instance, more than twenty oxides of iron vanadate such as $Fe_{0.1}V_2O_{5.15}$, $Fe_{0.33}V_2O_5$, $Fe_{0.83}V_{1.17}O_4$, $Fe_2V_2O_5$, $Fe_2V_4O_{12.29}$, $Fe_2V_4O_{13}$, FeV_2O_6, FeV_3O_8, $FeVO_3$, Fe_2VO_4, FeV_2O_4, $FeVO_4$, and $Fe_4V_6O_{21}$. have been reported [3–6], and their potential application in rechargeable batteries, electrical and optical switching devices, and heterogeneous catalysis fields have also been investigated [7,8].

Among the reported iron vanadate oxides, the oxides Fe_2VO_4 and FeV_2O_4 have been the focus of special attention [9,10] because they possess a spinel structure and key structural-related magnetic or electrical properties [11,12]. Fe_2VO_4 has the inverse spinel structure of $Fe^{3+}[Fe^{2+}V^{3+}]O_4$, like magnetite $Fe^{3+}[Fe^{2+}Fe^{3+}]O_4$. However, FeV_2O_4 changes to the normal spinel structure of $Fe^{2+}[V^{3+}]_2O_4$ with divalent iron (Fe^{2+}) occupying tetrahedral sites and trivalent vanadium (V^{3+}) occupying octahedral sites due to the strong affinity of V^{3+} ions for octahedral sites.

In addition to the stoichiometric compounds Fe_2VO_4 and FeV_2O_4, a complete solid solution $Fe_{3-x}V_xO_4$ can be formed by $Fe^{3+}[Fe^{2+}Fe^{3+}]O_4$ and $Fe^{2+}[V^{3+}]_2O_4$. The cation distribution in the spinel solid solution $Fe_{3-x}V_xO_4$ has been determined by Mössbauer spectroscopy [13]. For $0 < x < 1.0$, the solid solution remains an inverse spinel structure as $Fe^{3+}[Fe^{2+}Fe^{3+}{}_{1-x}V^{3+}{}_x]O_4$. For $1.64 < x < 2.0$, the solid solution remains a normal spinel structure as $Fe^{2+}[Fe^{3+}{}_{1-x/2}V^{3+}{}_{x/2}]_2O_4$. The transition from normal to inverse is observed for $1.0 < x < 1.64$.

Due to the similar structure to magnetite Fe_3O_4, great consideration has been given to the magnetic properties of $Fe_{3-x}V_xO_4$. Wakihara et al. [14] synthesized the spinel solid solution with stoichiometric composition at 1500 K under controlled CO_2–H_2 atmospheres, measured the Curie temperature and the magnetization behaviors of a series of solid-solution compounds, and proposed a magnetic structure model. Jin et al. [15] fabricated epitaxial $Fe_{3-x}V_xO_4$ ($0 \leq x \leq 0.6$) films by using reactive co-sputtering from pure Fe and V in a gas mixture of Ar and O_2, and the magnetic and magnetotransport properties of the film spinels were studied at room temperature. Pool et al. [16] synthesized nanoparticles of $Fe_{3-x}V_xO_4$ with up to 33% vanadium substitution (x = 0 to 1) by mixing appropriate ratios of solutions of 0.5 mmol $V(acac)_3$ and $Fe(acac)_3$, 1,2-hexadecanediol with benzyl ether, oleic acid(1.5 mmol), and oleylamine (1.5 mmol) under evacuated conditions. The site preference of the vanadium and the magnetic behavior of the nanoparticles were investigated through L23edge X-ray absorption spectroscopy (XAS) and X-ray magnetic circular dichroism (MCD) spectra.

Research on the optical absorption properties as well as the catalytic and stable properties of $Fe_{3-x}V_xO_4$ have also been reported. Kim et al. [17] prepared the $Fe_{3-x}V_xO_4$ thin film on Si (100) substrates by using a sol–gel method. The valence and occupying sites of V ions in the $Fe_{3-x}V_xO_4$ ($x < 1.0$) compounds were revealed by using X-ray diffraction, X-ray photoelectron spectroscopy, and Mössbauer spectroscopy, while the optical absorption properties of the films were measured by spectroscopic ellipsometry (SE). Häggblad et al. [18] investigated the catalytic effect of $Fe_{3-x}V_xO_4$ ($x < 1.37$) on the oxidation of methanol to produce formaldehyde, and the valence change of V ion was revealed by in and ex situ analyses of the samples with X-ray absorption near edge structure (XANES) spectroscopy.

Apart from the research on the physical properties of $Fe_{3-x}V_xO_4$, a number of works relating to the phase equilibria of $Fe_{3-x}V_xO_4$ have been carried out. Coetsee et al. [19] determined the existing phases with the change of Fe/V molar ratio in the V_2O_3–FeO system from 1673 K to 1873 K by using CO/CO_2 = 3 gas mixture to control the oxygen partial pressure. Wakihara et al. [20] determined the phase equilibria in FeO–Fe_2O_3–V_2O_3 system at 1500 K by varying the oxygen partial pressure and proposed the phase boundaries of $Fe_{3-x}V_xO_4$. In our previous publication [21], the phase equilibria of the FeO–V_2O_3 system at 1473 K under various oxygen partial pressures were determined, and a phase diagram of $\lg(p_{O_2}/atm)$ vs. the molar ratio of V/(Fe + V) was presented. Based on the available phase equilibria and thermodynamic data, the Fe–V–O system was assessed and optimized through the CALPHAD method. Xie et al. [2] performed the assessment by adopting the modified quasichemical model to describe the liquid phase in the system and the sublattice model based on the compound energy formalism to describe the spinel solid solution $Fe_{3-x}V_xO_4$. Du et al. [22] also performed an evaluation and modeling of the system by using the modified quasichemical model to describe the liquid oxide solution and the two sublattice spinel solution model within the framework of the compound energy formalism to the spinel solid solution $Fe_{3-x}V_xO_4$. In addition, the modeling works of some more complex systems, such as the Fe–Ti–V–O system [23] and CaO–FeO–Fe_2O_3–MgO–SiO_2-containing V_2O_3 and V_2O_5 system [24], were reported.

However, regarding the elementary thermodynamic data, i.e., the standard Gibbs energy of $Fe_{3-x}V_xO_4$, only the data of FeV_2O_4 was reported. The first Gibbs energy measurement was performed by Chipman and Dastur [25] by the equilibration of FeV_2O_4 with liquid Fe–V solution under a controlled H_2–H_2O gas atmosphere at 1873 K. Wakihara et al. [20] determined the standard Gibbs energy of the reaction of Fe + V_2O_3 + $0.5O_2$ = FeV_2O_4 and $0.05Fe + V_2O_3 + Fe_{0.95}O = FeV_2O_4$ at 1500 K, according to the equilibrated oxygen partial pressure. And even in the database of commercial thermodynamic software FactSage [26], only the data of FeV_2O_4 can be retrieved. Therefore, the present study aimed at providing the fundamental thermodynamic data of $Fe_{3-x}V_xO_4$ and understanding the effect of V substituting on the thermodynamic property of the spinel phase; the standard Gibbs energy of formation of $Fe_{3-x}V_xO_4$ was determined by combining theoretical derivation with experimental measurements.

2. Principle and Experimental

2.1. Principle of Determining the Gibbs Energy of $Fe_{3-x}V_xO_4$

The molar Gibbs energy of $Fe_{3-x}V_xO_4$ can be calculated according to Equation (1).

$$G_{Fe_{3-x}V_xO_4} = (3-x)\mu_{Fe} + x\mu_V + 2\mu_{O_2} \quad (1)$$

where μ_{Fe}, μ_V, and μ_{O_2} are the chemical potentials of Fe, V, and O_2, respectively. Furthermore, according to the Gibbs–Duhem relation [27], the chemical potentials of Fe, V, and O_2 can be connected by Equation (2).

$$(3-x)\cdot d\mu_{Fe} + x\cdot d\mu_V + 2\cdot d\mu_{O_2} = 0 \quad (2)$$

If the oxygen partial pressure is fixed unchangeably, the $d\mu_{O_2}$ will be zero, and then Equation (2) can be simplified as Equation (3).

$$(3-x)\cdot d\mu_{Fe} + x\cdot d\mu_V = 0 \quad (3)$$

Then, Equation (4) can be obtained by dividing both sides of Equation (3) by x.

$$d\mu_V = -\frac{3-x}{x} d\mu_{Fe} \quad (4)$$

where $\frac{3-x}{x}$ represent the molar ratio of Fe to V in $Fe_{3-x}V_xO_4$. If it is replaced by y, Equation (4) becomes Equation (5).

$$d\mu_V = -y\cdot d\mu_{Fe} \quad (5)$$

By integrating Equation (5) from y_s to y, the following relations can be obtained.

$$\int_{\mu_{V,y_s}}^{\mu_V} d\mu_V = \int_{y_s}^{y} -y\cdot d\mu_{Fe} \quad (6)$$

where y_s refers to the molar ratio of Fe to V in $Fe_{3-x}V_xO_4$ when it is saturated or equilibrated with V_2O_3, i.e., the minimum molar ratio of Fe to V in $Fe_{3-x}V_xO_4$ at the fixed oxygen partial pressure. Correspondingly, μ_{V,y_s} refers to the chemical potential of V in the $Fe_{3-x}V_xO_4$ that is saturated or equilibrated with V_2O_3 at the fixed oxygen partial pressure.

Next, using the method of integration by parts, Equation (6) can be changed to Equation (7).

$$\mu_V - \mu_{V,\ y_s} = [-y\cdot\mu_{Fe}]_{y_s,\mu_{Fe,y_s}}^{y,\mu_{Fe}} + \int_{y_s}^{y} \mu_{Fe}\cdot dy \quad (7)$$

Rearranging Equation (7), a relation of Equation (8) can be obtained.

$$\mu_V = \mu_{V,\ y_s} + (y_s\cdot\mu_{Fe,y_s} - y\cdot\mu_{Fe}) + \int_{y_s}^{y} \mu_{Fe}\cdot dy \quad (8)$$

Equation (8) tells us if we can know the functional relationship between μ_{Fe} and y, as well as the value of y_s and $\mu_{V,\ y_s}$, then the chemical potential of V in $Fe_{3-x}V_xO_4$ can be calculated through Equation (8).

Regarding the parameters y_s and $\mu_{V,\ y_s}$, they can be determined by using the following approaches. For y_s, it can be read directly from the phase diagram of the Fe_tO–V_2O_3 system at 1473 K under various oxygen partial pressures, which we have reported in a previous publication [21]. For $\mu_{V,\ y_s}$, it can be determined by the formation reaction of V_2O_3 shown as Equation (9), because the chemical potentials of V in all the equilibrated phases are equal.

$$V + 3/4O_2 = 1/2V_2O_3 \quad (9)$$

According to Equation (9), the $\mu_{V,\ y_s}$ can be determined by Equation (10).

$$\mu_{V,\ y_s} = 1/2\mu^{\theta}_{V_2O_3} - 3/4\left[\mu^{\theta}_{O_2} + RTln\left(p_{O_2}/p^{\theta}\right)\right] \quad (10)$$

where $\mu^{\theta}_{V_2O_3}$ is the chemical potential of pure V_2O_3 compound, $\mu^{\theta}_{O_2}$ is the chemical potential of O_2 at 1atm, and p_{O_2} is the oxygen partial pressure adopted in experiments.

From the above analysis, it can be concluded that when the dependence of μ_{Fe} on y can be obtained, the μ_V will be calculated through Equation (8), and the $G_{Fe_{3-x}V_xO_4}$ (molar Gibbs energy of $Fe_{3-x}V_xO_4$) can be calculated by inserting μ_V and μ_{Fe} into Equation (1). Therefore, to measure the μ_{Fe} in $Fe_{3-x}V_xO_4$ is a prerequisite for the determination of the molar Gibbs energy of $Fe_{3-x}V_xO_4$.

2.2. Experimental Procedure for Measuring μ_{Fe} in the Solid-Solution Phase $Fe_{3-x}V_xO_4$

The experiments to measure the values of the chemical potential of Fe in the solid solution phase $Fe_{3-x}V_xO_4$ consisted of three steps. The first was to prepare the pure $Fe_{3-x}V_xO_4$ compounds with different Fe/V molar ratios at fixed oxygen partial pressure; the second was to equilibrate the prepared $Fe_{3-x}V_xO_4$ with liquid copper; the third was to measure the content of Fe in the copper by Inductive Coupled Plasma–Optical Emission Spectrometer (ICP–OES, OPTIMA 7000DV, Waltham, MA, USA).

Pure $Fe_{3-x}V_xO_4$ compounds with different Fe/V molar ratios were prepared through the conventional solid-state reaction method under CO–CO_2 gas mixture atmosphere at 1473 K, where CO–CO_2 gas mixture was adopted to control the oxygen partial pressure in the reaction chamber. The experimental apparatus and the operating details can be found in our previous publications [21,28,29]. The reactants, composed of analytical reagents of Fe, Fe_2O_3, and V_2O_3 with purity of 99.99%, were ground homogeneously in an agate mortar and pressed into pellets. Then, the pellets were placed into an alumina crucible and reacted in a pre-designed atmosphere for 72 h. Detailed information about the composition of prepared samples and the preparing atmospheres is shown in Table 1.

Table 1. Composition and preparing conditions of $Fe_{3-x}V_xO_4$ compounds.

No. of Samples	Fe/V Molar Ratio	Volume Ratio of CO to CO_2	Oxygen Partial Pressure (atm)
1-1	1.6	2	2.39×10^{-12}
1-2	1.4		
1-3	1.2		
1-4	1.0		
1-5	0.8		
1-6	0.6		
2-1	1.8	1	9.57×10^{-12}
2-2	1.6		
2-3	1.4		
2-4	1.2		
2-5	1.0		
2-6	0.8		
3-1	2.8	0.5	3.83×10^{-11}
3-2	2.6		
3-3	2.2		
3-4	2.0		
3-5	1.6		
3-6	1.0		

After the pure $Fe_{3-x}V_xO_4$ was prepared, it was equilibrated with liquid copper at 1473 K for 72 h under the same atmosphere as the preparing condition. Here, the liquid copper was selected as the metal to equilibrate with the $Fe_{3-x}V_xO_4$ sample. This is because the liquid copper is stable and cannot be oxidized during the present investigated oxygen partial pressure range (2.39×10^{-12}~3.83×10^{-11} atm), and also, the activity coefficient of Fe in liquid copper is far greater than unity [30], which can ensure that the concentration of Fe in liquid copper is very small. For a typical run of the equilibrating experiment, about 5 g copper powder with a purity of 99.99% was placed into an alumina crucible, a tablet of about 2.5 g of $Fe_{3-x}V_xO_4$ was placed above the copper powder, and then the crucible containing the samples was put into a furnace and heated to 1473 K. When the temperature reached 1473 K, the samples were held for 72 h to ensure the equilibrium between $Fe_{3-x}V_xO_4$ and liquid copper. Then, the equilibrated samples were quenched by lifting the sample from the high-temperature zone to the water-cooled quenching chamber. The quenched sample was taken out from the quenching chamber, and the solidified copper was separated from the $Fe_{3-x}V_xO_4$ by a mechanical method. Then, the surface of the separated copper was cleaned mechanically for ICP–OES analysis to measure the content of Fe. For the ICP–OES analysis of Fe content, each sample was measured three times to ensure the error was less than 10 ppm; then, the measured three values were averaged as the final results.

When the content of Fe in the copper sample was measured, the chemical potential of Fe in the $Fe_{3-x}V_xO_4$ sample can be deduced by using the following method. As the $Fe_{3-x}V_xO_4$ sample was equilibrated with the liquid copper chemically, the chemical potential of Fe in the $Fe_{3-x}V_xO_4$ sample was equal to that in the copper sample. So, by using the measured content of Fe in copper, the chemical potential of Fe can be determined by Equation (11).

$$\mu_{Fe} = \mu_{Fe}^{\theta} + RTln\left(\gamma_{Fe(Cu)} \cdot x_{Fe(Cu)}\right) \quad (11)$$

where μ_{Fe}^{θ} is the chemical potential of pure iron, $\gamma_{Fe(Cu)}$ is the activity coefficient of Fe in liquid copper, and $x_{Fe(Cu)}$ is the molar fraction of Fe in the liquid copper. Furthermore, if the content of Fe in the liquid copper is low and can be treated as a dilute solution, the activity coefficient $\gamma_{Fe(Cu)}$ can be replaced by the Henry constant of Fe in liquid copper $\gamma_{Fe(Cu)}^{0}$, which was reported to be 24.1 relative to the pure solid Fe [30]. Therefore, in the present study, the chemical potential of Fe would be determined by Equation (12).

$$\mu_{Fe} = \mu_{Fe}^{\theta} + 1473 \cdot R \cdot ln\left(24.1 \cdot x_{Fe(Cu)}\right) \quad (12)$$

After μ_{Fe} in the $Fe_{3-x}V_xO_4$ sample with different Fe/V molar ratio was determined, the dependence of μ_{Fe} on y can be deduced. When the relationship between μ_{Fe} and y was obtained, the molar Gibbs energy of $Fe_{3-x}V_xO_4$ can then be obtained by the approach presented in the previous section.

3. Results and Discussion

3.1. Chemical Potential of Fe in the $Fe_{3-x}V_xO_4$ under Different Oxygen Partial Pressures

In our previous publication [21], the phase diagram of the "FeO"–V_2O_3 system at 1473 K in the oxygen partial pressure range of 5.98×10^{-15} atm to 2.39×10^{-8} atm was reported. Under the present investigated oxygen partial pressures, the Fe/V molar ratio for the single-phase area of $Fe_{3-x}V_xO_4$ is summarized in Table 2. Where y_L and y_s correspond to the maximal and minimum Fe/V molar ratio of $Fe_{3-x}V_xO_4$ single-phase area. When the Fe/V molar ratio in the system is larger than y_L, $Fe_{3-x}V_xO_4$ will coexist with the FeO phase. And when the Fe/V in the system is less than y_s, $Fe_{3-x}V_xO_4$ will coexist with the V_2O_3 phase.

Table 2. Compositional limitations of $Fe_{3-x}V_xO_4$ single-phase area.

Oxygen Partial Pressure	Compositional Limitations	
p_{O_2}/atm	y_s	y_L
2.39×10^{-12}	0.524	1.604
9.57×10^{-12}	0.565	2.300
3.83×10^{-11}	0.567	3.098

From Table 2, it can be clearly seen that the Fe/V ratio of the presently investigated samples is located in the single-phase area of $Fe_{3-x}V_xO_4$. So this can ensure the prepared compounds are pure phase with the pre-designed Fe/V molar ratio.

In Table 3, the ICP-OES measurement results for the contents of Fe in the quenched copper phase that had been equilibrated with $Fe_{3-x}V_xO_4$ are present. For the sake of clarity, the Fe/V molar ratio of the equilibrating $Fe_{3-x}V_xO_4$ compound and the equilibrating oxygen partial pressure are also listed together in Table 3. By using the measured contents of Fe in the quenched copper phase, the chemical potential of Fe in $Fe_{3-x}V_xO_4$ was calculated according to Equation (12), and the calculated values are shown in the form of $\mu_{Fe} - \mu_{Fe}^{\theta}$ in the last column of Table 3.

Table 3. The equilibrating experimental conditions and the related results.

Equilibrating Experimental Conditions			Results		
No.	y	p_{O_2}/atm	Mass % of Fe in Cu	$x_{Fe(Cu)}$	$\mu_{Fe}-\mu_{Fe}^{\theta}$ (J/mol)
1-1	1.6	2.39×10^{-12}	0.52	0.0059	−23,861.3
1-2	1.4		0.45	0.0051	−25,630.8
1-3	1.2		0.38	0.0043	−27,700.2
1-4	1.0		0.35	0.0040	−28,706.8
1-5	0.8		0.24	0.0027	−33,325.5
1-6	0.6		0.18	0.0020	−36,847.6
2-1	1.8	9.57×10^{-12}	0.41	0.0047	−26,770.1
2-2	1.6		0.36	0.0041	−28,362.0
2-3	1.4		0.31	0.0035	−30,192.4
2-4	1.2		0.24	0.0027	−33,325.5
2-5	1.0		0.15	0.0017	−39,079.9
2-6	0.8		0.08	0.0009	−46,777.0
3-1	2.8	3.83×10^{-11}	0.31	0.0035	−30,192.4
3-2	2.6		0.28	0.0032	−31,438.4
3-3	2.2		0.20	0.0023	−35,557.6
3-4	2.0		0.19	0.0022	−36,185.6
3-5	1.6		0.17	0.0019	−37,547.4
3-6	1.0		0.08	0.0009	−46,777.0

y is the molar ratio of Fe to V in $Fe_{3-x}V_xO_4$.

From the calculated results of $\mu_{Fe} - \mu_{Fe}^{\theta}$ shown in the last column of Table 3, it can be found that both the Fe/V molar ratio of $Fe_{3-x}V_xO_4$ and the equilibrating oxygen partial pressure have a significant effect on the chemical potential of Fe in the $Fe_{3-x}V_xO_4$ compound. At each fixed oxygen partial pressure, the chemical potential of Fe increased gradually with the increase of the Fe/V molar ratio. By comparing the results with the same Fe/V ratio, it can be found that the chemical potential of Fe decreased gradually with the increase of the equilibrating oxygen partial pressures. For instance, the $\mu_{Fe} - \mu_{Fe}^{\theta}$ for $Fe_{3-x}V_xO_4$(Fe/V = 1.6) decreased from −23,861.3 J/mol to −28,362.0 J/mol and then to −37,547.4 J/mol,

while the oxygen partial pressure increased from 2.39×10^{-12} atm to 9.57×10^{-12} atm and then to 3.83×10^{-11} atm.

In view of the above-indicated situation, it is an expedient approach to deduce the functional relations between μ_{Fe} and y separately at each experimental oxygen partial pressure. It was assumed that the relations between μ_{Fe} and y could be expressed by the relation shown in Equation (13).

$$\mu_{Fe} = \mu_{Fe}^{\theta} + RTln(a + by) \tag{13}$$

To determine the model parameters a and b, $\exp\left[\left(\mu_{Fe} - \mu_{Fe}^{\theta}\right)/\mathrm{RT}\right]$ was plotted against y, and the results are shown in Figure 1.

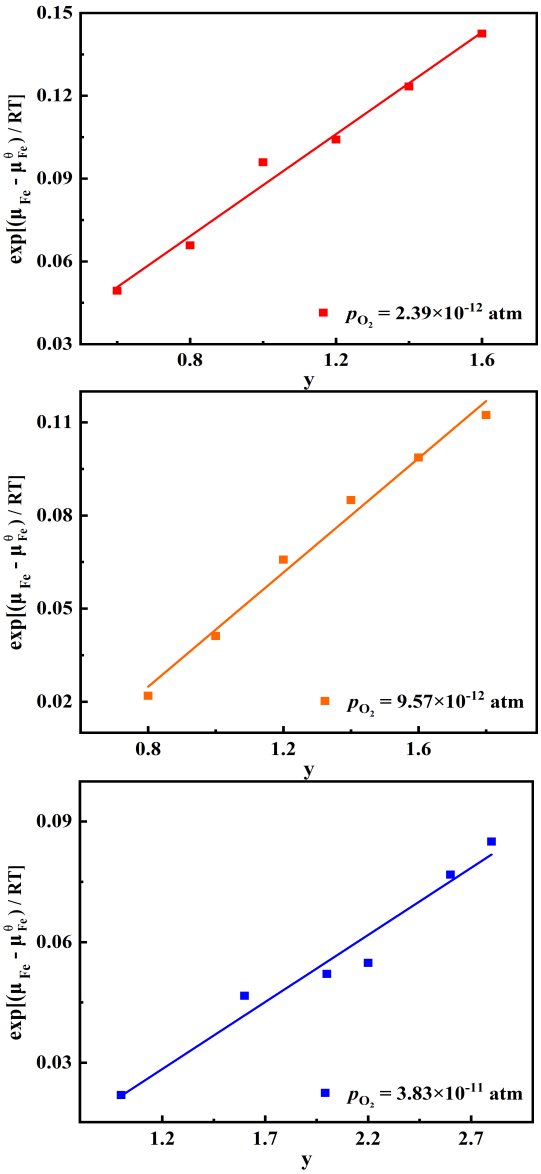


Figure 1. Plots of $\exp\left[\left(\mu_{Fe} - \mu_{Fe}^{\theta}\right)/\mathrm{RT}\right]$ against Fe/V ratio of $Fe_{3-x}V_xO_4$ and the linear fitting results.

From Figure 1, it can be seen that satisfactory linear relationships exist between $\exp\left[\left(\mu_{Fe} - \mu_{Fe}^{\theta}\right)/\mathrm{RT}\right]$ and y. This implies that the assumed functional relation by Equation (13) is acceptable in the current investigated conditions, and the obtained functional relations between μ_{Fe} and y at different oxygen partial pressures are summarized and presented in Table 4.

Table 4. The functional relations between μ_{Fe} and y at different oxygen partial pressure.

Equilibrating p_{O_2}/atm	Functional Relations between μ_{Fe} and y
2.39×10^{-12}	$\mu_{Fe} = \mu^{\theta}_{Fe} + RTln(-0.0048 + 0.092y)$
9.57×10^{-12}	$\mu Fe = \mu Fe\theta + RTln - 0.0488 + 0.092y$
3.83×10^{-11}	$\mu_{Fe} = \mu^{\theta}_{Fe} + RTln(-0.0116 + 0.033y)$

3.2. Chemical Potential of V in the $Fe_{3-x}V_xO_4$ under Different Oxygen Partial Pressure

After obtaining the functional relationships between the μ_{Fe} and y, the chemical potential of V in $Fe_{3-x}V_xO_4$ under different oxygen partial pressures were derived. The detailed procedure is as follows. Firstly, the functional relationship between μ_{Fe} and y, as shown in Equation (13), was inserted into Equation (8), yielding Equation (14).

$$\begin{array}{c}\mu_V = \mu_{V,\ y_s} + \left[y_s \cdot \left(\mu^{\theta}_{Fe} + RTln(a + by_s)\right) - y \cdot \left(\mu^{\theta}_{Fe} + RTln(a + by)\right)\right] \\ + \int_{y_s}^{y} \left(\mu^{\theta}_{Fe} + RTln(a + by)\right) \cdot dy\end{array} \quad (14)$$

Rearranging Equation (14), Equation (15) was obtained.

$$\mu_V = \mu_{V,\ y_s} + [y_s RTln(a + by_s) - yRTln(a + by)] + RT \int_{y_s}^{y} ln(a + by) \cdot dy \quad (15)$$

By integrating Equation (15) by parts, Equation (16) was obtained.

$$\begin{array}{c}\mu_V = \mu_{V,\ y_s} + [y_s RTln(a + by_s) - yRTln(a + by)] + [y \cdot RTln(a + by)]_{y_s}^{y} \\ -RT \int_{y_s}^{y} \left[1 - \frac{a}{(a+by)}\right] \cdot dy\end{array} \quad (16)$$

Equation (16) was rearranged and integrated again, and Equation (17) was obtained.

$$\mu_V = \mu_{V,\ y_s} - RT(y - y_s) + \left(\frac{a}{b}\right)[RTln(a + by)]_{y_s}^{y} \quad (17)$$

Then, inserting Equation (10) into Equation (17) yielded Equation (18)

$$\mu_V - \mu^{\theta}_V = \frac{1}{2}\Delta_f G^{\theta}_{V_2O_3} - 3/4RTln\left(p_{O_2}/p^{\theta}\right) - RT(y - y_s) + \left(\frac{a}{b}\right)RTln\left(\frac{a + by}{a + by_s}\right) \quad (18)$$

where $\Delta_f G^{\theta}_{V_2O_3}$ is the standard Gibbs energy of formation of V_2O_3, and its reported value at 1473 K is −864,690.7 J/mol. The values of y_s at 2.39×10^{-12} atm, 9.57×10^{-12} atm, and 3.83×10^{-11} are 0.524, 0.565, and 0.567, respectively.

Now, through Equation (18), the values of $\mu_V - \mu^{\theta}_V$ for $Fe_{3-x}V_xO_4$ with various Fe/V ratios under different oxygen partial pressures can be calculated. The calculated results are summarized and presented in Table 5.

Table 5. The derived $\mu_V - \mu^{\theta}_V$ as well as the measured $\mu_{Fe} - \mu^{\theta}_{Fe}$ in $Fe_{3-x}V_xO_4$ compounds.

Equilibrating Experimental Conditions			Results	
No.	***y***	p_{O_2}/atm	$\mu_{Fe}-\mu^{\theta}_{Fe}$ **(J/mol)**	$\mu_V-\mu^{\theta}_V$ **(J/mol)**
1-1	1.6	2.39×10^{-12}	−23,861.3	−200,496.5
1-2	1.4		−25,630.8	−197,958.8
1-3	1.2		−27,700.2	−195,406.8
1-4	1.0		−28,706.8	−192,835.2
1-5	0.8		−33,325.5	−190,234.6
1-6	0.6		−36,847.6	−187,586.3

Table 5. *Cont.*

Equilibrating Experimental Conditions			Results	
No.	y	p_{O_2}/atm	$\mu_{Fe}-\mu_{Fe}^{\theta}$ **(J/mol)**	$\mu_V-\mu_V^{\theta}$ **(J/mol)**
2-1	1.8	9.57×10^{-12}	−26,770.1	−237,836.0
2-2	1.6		−28,362.0	−234,273.1
2-3	1.4		−30,192.4	−230,479.1
2-4	1.2		−33,325.5	−226,331.9
2-5	1.0		−39,079.9	−221,577.7
2-6	0.8		−46,777.0	−215,523.2
3-1	2.8	3.83×10^{-11}	−30,192.4	−249,849.2
3-2	2.6		−31,438.4	−247,033.0
3-3	2.2		−35,557.6	−241,291.1
3-4	2.0		−36,185.6	−238,348.9
3-5	1.6		−37,547.4	−232,253.9
3-6	1.0		−46,777.0	−222,086.1

y is the molar ratio of Fe to V in $Fe_{3-x}V_xO_4$.

3.3. Standard Gibbs Energy of Formation of $Fe_{3-x}V_xO_4$ at 1473 K

According to the definition of standard Gibbs energy of formation, the standard Gibbs energy of $Fe_{3-x}V_xO_4$ can be determined by the following relation.

$$\Delta_f G^{\theta}_{Fe_{3-x}V_xO_4} = \mu^{\theta}_{Fe_{3-x}V_xO_4} - (3-x)\mu^{\theta}_{Fe} - x\mu^{\theta}_{V} - 2\mu^{\theta}_{O2} \quad (19)$$

where $\mu^{\theta}_{Fe_{3-x}V_xO_4}$, the chemical potential of pure $Fe_{3-x}V_xO_4$, is equal to the molar Gibbs energy of pure $Fe_{3-x}V_xO_4$, so Equation (1) can be inserted into Equation (19) to replace the $\mu^{\theta}_{Fe_{3-x}V_xO_4}$. Then, a relation shown as Equation (20) can be obtained.

$$\Delta_f G^{\theta}_{Fe_{3-x}V_xO_4} = (3-x)\left(\mu_{Fe} - \mu^{\theta}_{Fe}\right) + x\left(\mu_V - \mu^{\theta}_V\right) + 2\left(\mu_{O_2} - \mu^{\theta}_{O2}\right) \quad (20)$$

Furthermore, according to the relationship between μ_{O_2} and oxygen partial pressure, Equation (20) can be changed to Equation (21).

$$\Delta_f G^{\theta}_{Fe_{3-x}V_xO_4} = (3-x)\left(\mu_{Fe} - \mu^{\theta}_{Fe}\right) + x\left(\mu_V - \mu^{\theta}_V\right) + 2RTln\left(p_{O_2}/p^{\theta}\right) \quad (21)$$

Now, by inserting the values of $\mu_{Fe} - \mu^{\theta}_{Fe}$ and $\mu_V - \mu^{\theta}_V$ presented in Table 4 into Equation (21), the standard Gibbs energy of formation of $Fe_{3-x}V_xO_4$ with different Fe/V ratios under experimental oxygen partial pressures was calculated, and the calculated results are listed in Table 6.

Table 6. The standard Gibbs energy of formation of $Fe_{3-x}V_xO_4$.

No.	y	p_{O_2}/atm	$\Delta_f G^{\theta}_{Fe_{3-x}V_xO_4}$ **J/mol**
1-1	1.6	2.39×10^{-12}	−930,820.9
1-2	1.4		−947,729.6
1-3	1.2		−967,218.6
1-4	1.0		−987,740.2
1-5	0.8		−1,016,918.9
1-6	0.6		−1,048,605.1

Table 6. *Cont.*

No.	y	p_{O_2}/atm	$\Delta_f G^{\theta}_{Fe_{3-x}V_xO_4}$ J/mol
2-1	1.8	9.57×10^{-12}	−927,899.3
2-2	1.6		−944,122.7
2-3	1.4		−962,382.6
2-4	1.2		−984,614.1
2-5	1.0		−1,012,433.4
2-6	0.8		−1,043,021.7
3-1	2.8	3.83×10^{-11}	−851,470.1
3-2	2.6		−861,457.0
3-3	2.2		−887,027.6
3-4	2.0		−898,199.8
3-5	1.6		−924,783.2
3-6	1.0		−990,774.3

y is the molar ratio of Fe to V in $Fe_{3-x}V_xO_4$.

To further understand the influence of Fe/V ratio and oxygen partial pressure on the standard Gibbs energy of formation of $Fe_{3-x}V_xO_4$, the calculated values presented in Table 5 were demonstrated in Figure 2 by plotting the $\Delta_f G^{\theta}_{Fe_{3-x}V_xO_4}$ against the Fe/V molar ratio. From Figure 2, it can be seen apparently that the data of $\Delta_f G^{\theta}_{Fe_{3-x}V_xO_4}$ determined under different oxygen partial pressures shown not only very similar changing trends but also very small differences. This implies that in the present investigated composition and atmosphere ranges, the standard Gibbs energy of formation of $Fe_{3-x}V_xO_4$ is mainly influenced by the Fe/V molar ratio, and the effect of oxygen partial pressure is almost negligible.

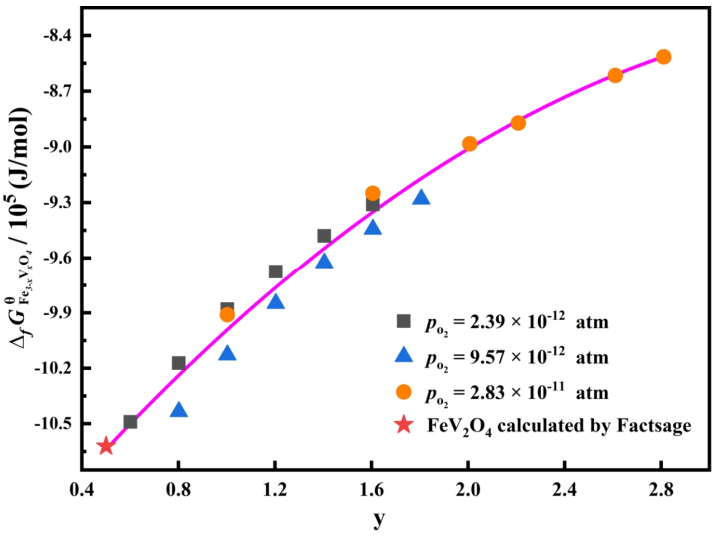


Figure 2. The changing trend of $\Delta_f G^{\theta}_{Fe_{3-x}V_xO_4}$ with Fe/V ratio under different oxygen partial pressures.

In Figure 2, apart from the data determined in the present study, the standard Gibbs energy of formation of FeV_2O_4 reported as −1,061,678.1 J/mol at 1473 K [26] was also denoted by using a star marker. It can be found that the $\Delta_f G^{\theta}_{FeV_2O_4}$ shows excellent agreement and compatibility with the present determined data.

From Figure 2, although the trend of the change of the standard Gibbs energy of formation of $Fe_{3-x}V_xO_4$ with the increasing of Fe/V molar ratio can be seen explicitly, the functional relationship between them is implicit. To derive it, the standard Gibbs energies of

the formation of FeV_2O_4 and Fe_3O_4 were considered because $Fe_{3-x}V_xO_4$ can be considered as a complete solid solution formed with FeV_2O_4 and Fe_3O_4 FeV_2O_4 and Fe_3O_4 as the end members.

In Figure 3, the standard Gibbs energies of the formation of FeV_2O_4 and Fe_3O_4 were plotted together with that of $Fe_{3-x}V_xO_4$ against $x/2$. Where $x/2$ can be regarded as the molar fraction of the end member FeV_2O_4. The adopted data of the standard Gibbs energies of the formation of Fe_3O_4 were –648765.3 J/mol [26].

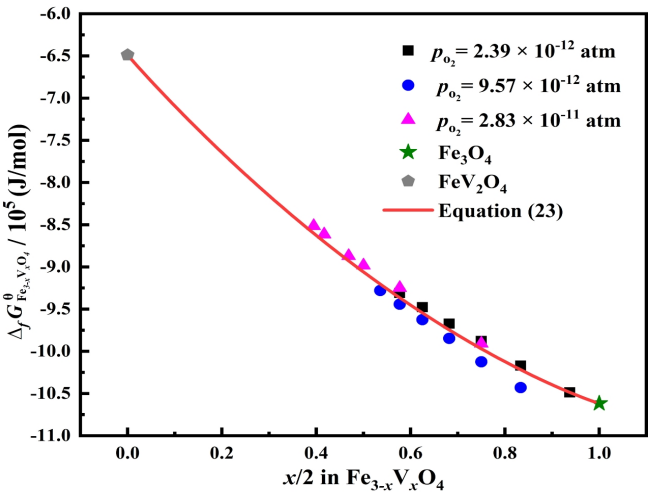


Figure 3. Comparing the present determined $\Delta_f G^{\theta}_{Fe_{3-x}V_xO_4}$ with the model calculating results.

From Figure 3, it can be seen that the present determined standard Gibbs energy of formation of $Fe_{3-x}V_xO_4$ has high relevance with that of their end members. Therefore, the regular solution model was adopted tentatively to establish a calculating model of the standard Gibbs energy of formation of $Fe_{3-x}V_xO_4$.

According to the regular solution model, the Gibbs energy of a solution composed of A and B can be expressed by Equation (22).

$$G_{A-B} = x_A G^{\theta}_A + x_B G^{\theta}_B + x_A RTlnx_A + x_B RTlnx_B + \Omega x_A x_B \quad (22)$$

where G^{θ}_A and G^{θ}_B are Gibbs energy of pure components A and B, x_A and x_B are molar fractions of A and B, and Ω is the model parameter obtained from experimental data. In the present study, by using Fe_3O_4 to replace A, FeV_2O_4 to replace B, and fitting the model to the determined values of $\Delta_f G^{\theta}_{Fe_{3-x}V_xO_4}$, the following expression of calculating the standard Gibbs energy of formation of $Fe_{3-x}V_xO_4$ was obtained.

$$\begin{aligned}\Delta_f G^{\theta}_{Fe_{3-x}V_xO_4}(J/mol) &= (1-x/2)\Delta_f G^{\theta}_{Fe_3O_4} + (x/2)\Delta_f G^{\theta}_{FeV_2O_4} \\ &+(1-x/2)RTln(1-x/2) + (x/2)RTln(x/2) \\ &-168627.48(1-x/2)(x/2)\end{aligned} \quad (23)$$

To evaluate the estimating effect of the derived model, Equation (23) was used to calculate the $\Delta_f G^{\theta}_{Fe_{3-x}V_xO_4}$ with the x ranging from 0 to 2, and the calculated results are presented in Figure 3 using a solid line. By comparing the calculated values with that determined experimentally, it can be seen apparently that the derived model can estimate the standard Gibbs energy of formation of $Fe_{3-x}V_xO_4$ satisfactorily.

4. Conclusions

In view of the lack of primary thermodynamic data for the solid-solution compound $Fe_{3-x}V_xO_4$, an approach of determining the standard Gibbs energy of formation of

$Fe_{3-x}V_xO_4$ was proposed, and its applicability was confirmed. The detailed procedure of the approach and the obtained results are as follows:

1. The approach of determining $\Delta_f G^{\theta}_{Fe_{3-x}V_xO_4}$ consists of two steps. The first is to measure the chemical potential of Fe (μ_{Fe}) in $Fe_{3-x}V_xO_4$ under fixed oxygen partial pressure by using liquid copper as the equilibrating phase, thereby obtaining the composition-dependent relation of μ_{Fe}. The second is to calculate the $\Delta_f G^{\theta}_{Fe_{3-x}V_xO_4}$ by utilizing the Gibbs–Duhem relation.
2. The standard Gibbs energies of the formation of a variety of $Fe_{3-x}V_xO_4$ compounds were determined through this approach, and its reliability was verified by comparing the determined $\Delta_f G^{\theta}_{Fe_{3-x}V_xO_4}$ with the reported value of FeV_2O_4.
3. In the oxygen partial pressure range from 2.39×10^{-12} to 3.83×10^{-11} atm, the standard Gibbs energies of formation of $Fe_{3-x}V_xO_4$ is mainly decided by the Fe/V molar ratio and almost not related to the oxygen partial pressure.
4. The standard Gibbs energies of the formation of $Fe_{3-x}V_xO_4$ can be modeled satisfactorily using the regular solution model with Fe_3O_4 and FeV_2O_4 as the solution end members.

Author Contributions: Conceptualization, B.Y.; investigation, Q.M. and M.L.; writing—original draft preparation, Q.M. and M.L.; writing—review and editing, B.Y.; project administration, B.Y. All authors have read and agreed to the published version of the manuscript.

Funding: This research was funded by the State Key Laboratory of Vanadium and Titanium Resources Comprehensive Utilization grant number 2021P4FZG01A, and the National Natural Science Foundation of China, grant number 52174274.

Data Availability Statement: Not applicable.

Conflicts of Interest: The authors declare that they have no conflict of interest.

References

1. Lu, R.W.; Ren, X.L.; Zhan, C.Z.; Wang, C.; Lv, R.; Shen, W.; Kang, F.; Huang, Z.-H. Facile synthesis of FeVO@C materials as high-performance composite cathode for lithium-ion hybrid capacitor. *J. Alloys Compd.* **2020**, *835*, 155398. [CrossRef]
2. Xie, W.; Xin, X.R.; Cao, Z.M. Thermodynamic assessment of the Fe–V–O system. *CALPHAD Comput. Coupling Phase Diagr. Thermochem.* **2020**, *71*, 102213. [CrossRef]
3. Li, S.-R.; Ge, S.-Y.; Qiao, Y.; Chen, Y.-M.; Feng, X.-Y.; Zhu, J.-F.; Chen, C.-H. Three-dimensional porous $Fe_{0.1}V_2O_{5.15}$ thin film as a cathode material for lithium ion batteries. *Eectrochimica Acta* **2012**, *64*, 81–86. [CrossRef]
4. Xie, W.; Xin, X.R.; Cao, Z.M. Thermodynamic, lattice dynamical, and elastic properties of iron-vanadium oxides from experiments and first principles. *J. Am. Ceram. Soc.* **2020**, *103*, 3797–3811. [CrossRef]
5. Muller, J.; Joubert, J.C.; Marezio, M. The synthesis of the crystalline structure of the new oxide FeV_3O_8 ($Fe_xV_{1-x}O_2$, x = 0.25). *J. Solid State Chem.* **1979**, *27*, 191–199. [CrossRef]
6. Mawuse, A.A.; Song, N.; Jeong, I.H. All layered iron vanadate ($FeV_3O_9.2.1H_2O$) as electrode for symmetric supercapacitor application in aqueous electrolyte. *J. Alloys Compd.* **2023**, *938*, 168641.
7. Sharma, A.; Ashoka, S.; Nishchith, B.S.; Kalegowda, Y. Electrochemical quantification of glycine using amorphous iron vanadate nanoparticles modified pencil electrode. *Inorg. Chem. Commun.* **2023**, *153*, 110766. [CrossRef]
8. Zhang, C.L.; Sang, H.R.; Yang, H.P.; Hu, L.; Wu, B.; Yin, Y. Establishment of a novel Fenton-like enhanced low-temperature selective catalytic reduction over $FeVO_4$ catalysts. *J. Environ. Chem. Eng.* **2023**, *11*, 109634. [CrossRef]
9. Wang, D.Y.; Li, F.; Yan, B.J. Synthetic mechanism and kinetics of Fe_2VO_4 at 1273–1473 K from Fe_2O_3 and V_2O_3 under reducing atmosphere. *J. Alloys Compd.* **2019**, *797*, 1050–1058. [CrossRef]
10. Kawaguchi, S.; Ishibashi, H.; Nishihara, S.; Miyagawa, M.; Inoue, K.; Mori, S.; Kubota, Y. Anomalous magnetization behaviour in a single crystal of vanadium spinel FeV_2O_4. *J. Phys. Condens. Matter* **2013**, *25*, 416005. [CrossRef]
11. Cevik, E.; Bozkurt, A.; Gunday, S.T.; Qahtan, T.F.; Drmosh, Q.A.; Elsayed, K.A.; Akhtar, S.; Mustafa, A. Synthesis of NiO/Fe2VO4 nano-hybrid structures via sonication induced approach for electrochemical energy storage in non-aqueous medium. *J. Energy Storage* **2023**, *68*, 107873. [CrossRef]
12. Kang, J.S.; Hwang, J.; Kim, D.H.; Lee, E.; Kim, W.-J.; Kim, C.-S.; Kwon, S.; Lee, S.; Kim, J.; Ueno, T.; et al. Valence states and spin structure of spinel FeV2O4 with different orbital degrees of freedom. *Phys. Rev. B* **2012**, *85*, 165136. [CrossRef]
13. Abe, M.; Karachi, M.; Nomura, S. Mossbauer study of the FeV_2O_4–Fe_3O_4 system. *J. Solid State Chem.* **1974**, *10*, 351–356. [CrossRef]
14. Wakihara, M.; Shimizu, Y.; Katsura, T. Preparation and Magnetic properties FeV_2O_4–Fe_3O_4 system. *J. Solid State Chem.* **1971**, *3*, 478–483. [CrossRef]

15. Jin, C.; Liz, J.; Zheng, D.X.; Tang, M.; Li, P.; Bai, H. Effect of cation substitution on the magnetic and magnetotransport properties of epitaxial $Fe_{3-x}V_xO_4$ films. *Appl. Surf. Sci.* **2015**, *332*, 70–75. [CrossRef]
16. Pool, V.L.; Kleb, M.T.; Chorney, C.L.; Lee, J.H.; Park, J.Y.; Kim, S.J. Enhanced magnetization in $V_xFe_{3-x}O_4$ nanoparticles. *J. Magn. Magn. Mater.* **2015**, *396*, 304–307. [CrossRef]
17. Kim, K.J.; Choi, S.L.; Lee, H.J.; Lee, J.H.; Park, J.Y. Evolution of structural and optical-absorption properties in $V_xFe_{3-x}O_4$. *Solid State Commun.* **2007**, *143*, 285–288. [CrossRef]
18. Häggblad, R.; Massa, M.; Andersson, A. Stability and performance of supported Fe–V-oxide catalysts in methanol oxidation. *J. Catal.* **2009**, *266*, 218–227. [CrossRef]
19. Coetsee, T.; Pistorius, C. Preliminary Observations on Phase Relations in the "V_2O_3–FeO" and V_2O_3–TiO_2 Systems from 1400 °C to 1600 °C in Reducing Atmospheres. *J. Am. Ceram. Soc.* **2000**, *83*, 1485–1488. [CrossRef]
20. Wakihara, M.; Katsura, T. The Phase Equilibria in the FeO-Fe_2O_3-V_2O_3 System at 1500°K. *Bull. Chem. Soc. Jpn.* **1971**, *44*, 3043–3046. [CrossRef]
21. Yan, B.; Wang, D.; Qiu, Q.; Deng, T. Phase relations in the "FeO-V_2O_3" system at 1473 K and the magnetic properties of spinel phase $Fe_{3-x}V_xO_4$. *Ceram. Int.* **2020**, *46*, 6160–6167. [CrossRef]
22. Du, W.T.; Jung, I.H. Critical evaluation and thermodynamic modeling of the Fe-V-O (FeO-Fe_2O_3-VO-V_2O_3-VO-V_2O_5) system. *CALPHAD Comput. Coupling Phase Diagr. Thermochem.* **2019**, *67*, 101682. [CrossRef]
23. Malan, W.D.; Akdogan, G.; Taskinen, P.; Zietsman, J. Phase equilibria and thermodynamic evaluation of the Fe-Ti-V-O system in air. *CALPHAD Comput. Coupling Phase Diagr. Thermochem.* **2019**, *65*, 141–154. [CrossRef]
24. Jantzen, T.; Yazhenskikh, E.; Hack, K.; Baben, M.; Wu, G.; Müller, M. Addition of V_2O_5 and V_2O_3 to the CaO–FeO–Fe_2O_3–MgO–SiO_2 database for vanadium distribution and viscosity calculations. *CALPHAD Comput. Coupling Phase Diagr. Thermochem.* **2021**, *74*, 102284. [CrossRef]
25. Chipman, J.; Dastur, M.N. Vanadium-oxygen equilibrium in liquid iron. *JOM* **1951**, *191*, 111–115. [CrossRef]
26. The FactSage System. Available online: http://www.factsage.com/ (accessed on 1 July 2023).
27. Hillert, M. *Phase Equilibria, Phase Diagrams and Phase Transformations*, 2nd ed.; Cambridge University Press: Cambridge, UK, 2007; p. 49.
28. Wang, D.; Shu, Q.; Yan, B.; Wu, L.; Wang, J.; Dong, Y. Thermodynamics of the CaO–SiO_2–VO_x system at 1873 K under the oxygen partial pressure of 6.93×10^{-11} atm. *J. Am. Ceram. Soc.* **2017**, *100*, 4912–4927. [CrossRef]
29. Yan, B.; Wang, D.; Deng, T.; Wu, L.; Dong, Y. Effects of oxygen partial pressure on the thermodynamics of CaO–SiO_2–VO_x system at 1873 K. *J. Am. Ceram. Soc.* **2020**, *103*, 2114–2127. [CrossRef]
30. Sigworth, G.K.; Elliott, J.F. The thermodynamics of dilute liquid copper alloys. *Can. Metall. Q.* **1974**, *13*, 455–461. [CrossRef]

Disclaimer/Publisher's Note: The statements, opinions and data contained in all publications are solely those of the individual author(s) and contributor(s) and not of MDPI and/or the editor(s). MDPI and/or the editor(s) disclaim responsibility for any injury to people or property resulting from any ideas, methods, instructions or products referred to in the content.